JOURNAL OF STRUCTURAL ENGINEERING Vol.39 A (March 1993) JSCE

NUMERICAL SIMULATION AND EXPERIMENTAL STUDY OF DEEPER-WATER TLD IN THE PRESENCE OF SCREENS

By Zhongshan ZHAO* and Yozo FUJINO**

ABSTRACT

This paper deals with the numerical simulation and experimental study of deeper-water TLD. The term "deeper-water" is used to distinguish the depth-ratios adopted in this study from those of very shallow-water TLD. Metal screens are introduced to augment the lower damping accompanying deeper-water. The Boussinesq equations, which are suitable for weakly nonlinear, moderately long waves, are utilized to describe water motions in rectangular tanks driven horizontally to experience sinusoidal oscillations. The physical presence of screens is modelled mathematically with good accuracy provided that the extreme relative wave height at resonance is small and the agreements between predictions and observations are found to worsen with increasing wave height. The effects of water-depth ratio and screens as they alter the characteristics of TLD are clarified.

1. INTRODUCTION

TLD(Tuned Liquid Damper) has been investigated extensively in the field of structural engineering since its applications to ground structures was proposed in 1987[1].

Researches of TLD have, roughly speaking, followed two streams. Fujino[2], Sun[3] studied TLD with very shallow plain water. In their formulations of the equations of wave motion, the dispersion relation was implicitly represented in the scheme of discritization of the continuum governing equations. The number of divisions was, therefore, unfavorably linked to the water-depth ratio.

Noji et al [4,5] have experimentally explored TLD using deeper water. In their researches, metal screens were incorporated into the plain water TLD to augment the lower damping involved with deeper-water wave motions. Kaneko and Ishikawa[6] proposed a numerical model to include the effects of screens.

This paper deals with numerical simulation of wave motions inside a rectangular container installed with screens. Mathematical treatment of screens is essentially the same as addressed in [6]. The Boussinesq equations, which are suitable for weakly nonlinear, moderately long waves in shallow water, are here adopted to describe the physics of wave motions of concern, and they are solved by utilizing a finite difference scheme. Experimental observations are presented in a parallel way to facilitate comparisons and assessment of the numerical model.

* Research Engineer, Wind Engineering Institute(WEI), 5-18-12 Minami-Karasuyama, Setagaya-ku Tokyo157, Japan (Formerly Graduate Student, University of Tokyo)
** Professor, Department of Civil Engineering, University of Tokyo, Tokyo 113, Japan

2. GOVERNING EQUATIONS OF WAVE MOTION

A derivation of the governing Boussinesq equations is briefly described here for reference convenience[7]. The basic assumptions are that the flow is irrotational and a velocity potential exists.

We will limit the discussion to two-dimensional physics, though the extension to three-dimensional situation is straightforward. The fundamental conservation laws of liquid motion are adequately described, neglecting the damping force for the time being, by the Navier-Stokes equations:

$$\nabla \cdot \mathbf{u} = 0, \tag{1}$$

$$\left(\frac{\partial}{\partial t} + \mathbf{u}\cdot\nabla\right)\mathbf{u} = -\nabla\left(\frac{P}{\rho} + gz\right), \tag{2}$$

wherein $\mathbf{u}(\mathbf{x},t)$ is the velocity vector (u,w), u and w are the horizontal, vertical particle velocities, respectively, $P(\mathbf{x},t)$ the pressure, ρ the density, g the gravitational acceleration, t the time, and $\mathbf{x}=(x,z)$ with the z axis pointing vertically upward, as shown in Fig.1.

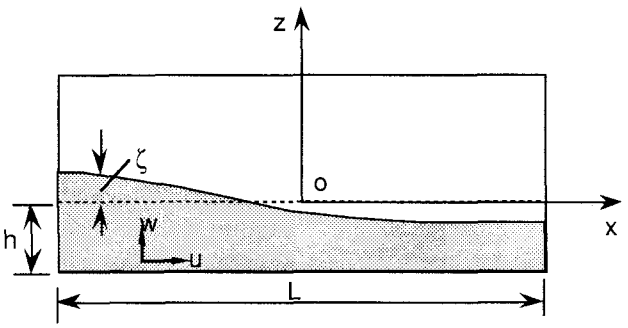

Fig.1 Sketch of definitions

For an irrotational flow, the velocity $\mathbf{u}(u,w)$ can be expressed as the gradient of a scalar potential Φ

$$\mathbf{u} = \nabla\Phi. \tag{3}$$

The introduction of Φ makes it possible to rewrite the two basic equations in terms of Φ to yield

$$\nabla^2\Phi = 0, \tag{4}$$

and

$$-\frac{P}{\rho} = gz + \frac{\partial\Phi}{\partial t} + \frac{1}{2}|\nabla\Phi|^2. \tag{5}$$

Boundary conditions are specified to obtain the governing equations. There are two kinds of boundary conditions, the kinematic boundary condition(KBC) and the dynamical boundary condition(DBC). The KBC on the free surface states the continuity of the air-water interface and it takes the form

$$\frac{\partial\zeta}{\partial t} + \frac{\partial\Phi}{\partial x}\frac{\partial\zeta}{\partial x} = \frac{\partial\Phi}{\partial z} \quad \text{on the free-surface} \tag{6}$$

where ζ is the wave height measured from the still water level. At the impenetrable solid bottom the KBC specifies that

$$\frac{\partial \Phi}{\partial z} = 0 \qquad \text{on } z = -h \tag{7}$$

wherein h is the still water-depth. On the air-water interface, both ζ and Φ are unknown and it is necessary to add a dynamical boundary condition concerning forces. Applying Eq. (2) on the free surface, we have

$$-\frac{P_a}{\rho} = g\zeta + \frac{\partial \Phi}{\partial t} + \frac{1}{2}|\nabla \Phi|^2 \quad \text{on } z = \zeta \tag{8}$$

where P_a is the atmospheric pressure which could be set to equal zero.

The governing equations (4),(6),(7) and (8) are to be nondimensionalized in the following manner:

$$x'=kx, \quad z'=\frac{z}{h}, \quad t'=k(gh)^{1/2}t$$

$$\zeta'=\frac{\zeta}{A}, \quad \Phi'=\Phi\left[\frac{A}{kh}(gh)^{1/2}\right]^{-1}, \tag{9}$$

in which k is the wave number and A is the characteristic wave height. The implied normalization on velocity components are

$$u = \frac{A}{h}(gh)^{1/2}u'$$
$$w = \frac{1}{kh}\frac{A}{h}(gh)^{1/2}w' \tag{10}$$

The difference in scaling for horizontal and vertical components is required by continuity. The normalized equations are

$$\mu^2(\Phi_{xx} + \Phi_{zz}) = 0, \qquad -1<z<\varepsilon\zeta \tag{11}$$

$$\mu^2[\zeta_t + \varepsilon\Phi_x\zeta_x] = \Phi_z, \qquad z=\varepsilon\zeta \tag{12}$$

$$\mu^2[\Phi_t + \zeta] + \frac{1}{2}\varepsilon[\mu^2\Phi_x^2 + \Phi_z^2] = 0, \qquad z=\varepsilon\zeta \tag{13}$$

$$\Phi_z = 0, \qquad z=-1. \tag{14}$$

with $\mu \equiv kh$ and $\varepsilon \equiv A/h$. They correspond to Eqs.(4), (6), (8) and (7), respectively. The primes have been dropped for simplicity.

For the time being we assume μ=kh is small, leaving ε to be arbitrary. Since Φ is analytical, it may be expanded as a power series in the vertical coordinate,

$$\Phi(x,z,t)=\sum_{n=0}^{\infty}(z+1)^n\Phi_n \tag{15}$$

where $\Phi_n = \Phi_n(x,t)$, n=0,1,2,3,..., whose orders of magnitude are yet unknown. The power series expansion of the velocity potential is more general and it is applicable to the situation of large ε. After substitution of Eq. (15) into Eq. (11), a recursive relation

$$\Phi_{n+2}=\frac{-\mu^2\nabla^2\Phi_n}{(n+1)(n+2)}, \qquad n=0,1,2,... \tag{16}$$

is obtained, from which we have

$$\Phi_1=\Phi_3=\Phi_5=0 \tag{17}$$

because of Eq.(14), which states that $\Phi_1=0$. Finally we have the expression

$$\Phi=\Phi_0-\frac{\mu^2}{2}(z+1)^2\nabla^2\Phi_0+\frac{\mu^4}{24}(z+1)^4\nabla^2\nabla^2\Phi_0+O(\mu^6). \tag{18}$$

Eq. (18) is then substituted into the free surface boundary conditions, Eqs. (12) and (13), to generate

$$\frac{1}{\varepsilon}H_t+\nabla H\cdot(\mathbf{u}_0-\frac{\mu^2}{2}H^2\nabla^2\mathbf{u}_0)+H\nabla\cdot\mathbf{u}_0 -\frac{\mu^2}{6}H^3\nabla^2(\nabla\cdot\mathbf{u}_0)=\mathbf{O}(\mu^4) \tag{19}$$

and

$$\frac{\partial\mathbf{u}_0}{\partial t}+\varepsilon\mathbf{u}_0\cdot\nabla\mathbf{u}_0+\nabla H/\varepsilon+\mu^2\nabla[-\frac{\varepsilon}{2}H^2\mathbf{u}_0\cdot\nabla^2\mathbf{u}_0 +\frac{\varepsilon}{2}H^2(\nabla\cdot\mathbf{u}_0)^2-\frac{1}{2}H^2\nabla\frac{\partial\mathbf{u}_0}{\partial t}]=O(\mu^4), \tag{20}$$

by defining $H=1+\varepsilon\zeta$ and $\mathbf{u}_0=\nabla\Phi_0$ as the horizontal velocity at the bottom.

In stead of $\mathbf{u}_0$, we may introduce the depth-averaged horizontal velocity $\bar{\mathbf{u}}$ defined by

$$\bar{\mathbf{u}}=\frac{1}{H}\int_{-1}^{\varepsilon\zeta}dz\nabla\Phi=\frac{1}{H}\int_{-1}^{\varepsilon\zeta}dz\nabla\Phi(\mathbf{u}_0-\frac{\mu^2}{2}(z+1)^2\nabla\nabla\cdot\mathbf{u}_0+\cdots) =\mathbf{u}_0-\frac{\mu^2}{6}H^2\nabla^2\mathbf{u}_0+\mathbf{O}(\mu^4), \tag{21}$$

which can be inverted to give

$$\mathbf{u}_0=\bar{\mathbf{u}}+\frac{\mu^2}{6}H^2\nabla^2\bar{\mathbf{u}}+\mathbf{O}(\mu^4). \tag{22}$$

After Eq. (22) is substituted into Eq. (19), it follows at once that

$$H_t+\varepsilon\nabla(H\bar{\mathbf{u}})=0 \tag{23}$$

which is just the depth-averaged law of continuity. In terms of $\bar{\mathbf{u}}$ Eq. (20) becomes

$$\bar{\mathbf{u}}_t + \varepsilon\bar{\mathbf{u}}\cdot\nabla\bar{\mathbf{u}} + \frac{\nabla H}{\varepsilon} + \frac{\mu^2}{6}(H^2\nabla^2\bar{\mathbf{u}})_t + \mu^2\nabla\{-\frac{\varepsilon}{3}H^2\,\bar{\mathbf{u}}\cdot\nabla^2\bar{\mathbf{u}} + \frac{\varepsilon}{2}H^2(\nabla\cdot\bar{\mathbf{u}})^2 - \frac{H^2}{2}\nabla\cdot\bar{\mathbf{u}}_t\} = \mathbf{O}(\mu^4). \tag{24}$$

Up to this point, the derivation is valid for arbitrary ε, and small μ=kh. Eqs. (23), (24) can be expressed in physical variables to be

$$H_t + \nabla\cdot(H\bar{\mathbf{u}}) = 0 \tag{25}$$

$$\bar{\mathbf{u}}_t + \bar{\mathbf{u}}\cdot\nabla\bar{\mathbf{u}} + g\nabla H + \frac{1}{6}(H^2\nabla^2\bar{\mathbf{u}})_t + \nabla\{-\frac{1}{3}H^2\,\bar{\mathbf{u}}\cdot\nabla^2\bar{\mathbf{u}} + \frac{1}{2}H^2(\nabla\cdot\bar{\mathbf{u}})^2 - \frac{H^2}{2}\nabla\cdot\bar{\mathbf{u}}_t\} = 0. \tag{26}$$

The pressure field may be obtained from Eq.(5), the Bernoulli's equation whose dimensionless form is

$$p = z + \varepsilon\{\Phi_t + \frac{\varepsilon}{2}[(\nabla\Phi)^2 + \frac{1}{\mu^2}\Phi_z^2]\}, \tag{29}$$

where p has been normalized by ρgh. The approximate pressure field, in dimensionless form, is

$$p = (\varepsilon\zeta - z) - \frac{\varepsilon\mu^2}{2}[H^2 - (z+1)^2]\{\nabla\cdot\frac{\partial\mathbf{u}_0}{\partial t} + \varepsilon[\mathbf{u}_0\cdot\nabla^2\mathbf{u}_0 - (\nabla\cdot\mathbf{u}_0)^2]\} + O(\mu^4), \tag{30}$$

or

$$p = \rho g(\zeta - z) - \frac{1}{2}[H^2 - (z+h)^2]\{\nabla\cdot\frac{\partial\bar{\mathbf{u}}}{\partial t} + \bar{\mathbf{u}}\cdot\nabla^2\bar{\mathbf{u}} - (\nabla\cdot\bar{\mathbf{u}})^2]\} + O(\mu^4), \tag{31}$$

in physical variables, using depth-averaged velocity $\bar{u}$.

For weakly nonlinear and moderately long waves in shallow water, Eqs. (25), (26) and (31) are approximated to include terms of order $O(\varepsilon)$ and $O(\mu^2)$ to produce, in physical variables,

$$\zeta_t + \nabla\cdot[(\zeta + h)\bar{\mathbf{u}}] = 0, \tag{32}$$

$$\bar{\mathbf{u}}_t + \varepsilon\,\bar{\mathbf{u}}\cdot\nabla\bar{\mathbf{u}} + \nabla\zeta - \frac{\mu^2}{3}\nabla\nabla\cdot\bar{\mathbf{u}}_t = 0, \tag{33}$$

and

$$p = \rho g(\zeta - z) + \frac{\rho}{2}(2zh + z^2)\nabla\cdot\bar{\mathbf{u}}_t. \tag{34}$$

Equations.(32), (33) and (34) are called the Boussinesq equations. They are applicable to describing wave motions under the conditions that $\varepsilon<1.0$ and $\mu<1.0$, and within these limitations their accuracy decreases with increasing wave height.

3. MODELLING OF THE PHYSICAL PRESENCE OF SCREENS

The damping of water sloshing is essential to a TLD's performances as an effective damper. Damping has been ignored in the derivation of the governing equations. In the following discussion, however, a linear damping term accounting for the viscosity of plain water will be incorporated into Eq. (33) to complete the formulation. The momentum equation in the horizontal direction we actually use in the numerical simulation is obtained simply by adding a linear damping term, $\lambda\mathbf{u}$, and an external excitation term, $\ddot{x}_s$, to Eq.(33). This leads to

$$\bar{u}_t + \varepsilon\,\bar{u}\cdot\nabla\bar{u} + \nabla\zeta - \frac{\mu^2}{3}\nabla\nabla\cdot\bar{u}_t + \lambda\,\bar{u}=\ddot{x}_s, \tag{33'}$$

in which λ is coefficient of linear damping and it is a function of the tank size, the viscosity and the frequency of water sloshing[9], or specifically

$$\lambda=k(2\nu\omega)^{1/2}\{1+(L/B)+\pi[1-(2h/L)]\mathrm{cosech}(2\pi h/L)+\frac{\pi}{2}\coth(\pi h/L)\} \tag{35}$$

for water sloshing inside a rectangular tank of dimension LxBxh, where L is the tank length in the x direction, B the width and h the still water-depth, k the wave number, ν the kinematic viscosity of water, ω the circular frequency of water oscillation [9].

The damping effects of screens are first addressed briefly before we continue to state the modelling of the physical presence of screens.

Simply speaking, damping causes energy dissipation. Energy dissipation due to fluid friction or viscosity happens all the time, inside the whole fluid body when and where the liquid sloshes. The presence of a metal screen, nevertheless, results in local energy dissipation while the fluid is passing through it. An immediate energy loss takes place there and this leads to a water-head loss. The value of head-loss is considered to be a function of the property of the screen, the flow state in the neighborhood of the screen and the Reynolds number, it can be evaluated empirically[8].

There is a parameter termed the coefficient of hydraulic resistance, δ, that links the head-loss quantitatively to flow state near the screen. δ itself is a function of the property of the screen only. The quantity of water-head loss is determined from expression

$$\Delta\zeta = \frac{\delta(\frac{1}{2}\rho U^2)}{\rho g} \tag{36}$$

in which U is the velocity of water passing the screen.

For screens made of circular metal wires, the resistance coefficient is, according to I.E. Idelchik[8],

$$\delta = k_0(1-\bar{f}) + (\frac{1}{\bar{f}}-1)^2, \qquad (Re>10^3) \tag{37}$$

$$\delta = k'_{Re}\,\delta_{eq}, \qquad (50<Re<10^3) \tag{38}$$

$$\delta = \frac{22}{Re} + \delta_{eq}, \qquad (Re<50) \tag{39}$$

where k_0=1.3(for conventional neither rusty nor dusty metal wires); $\bar{f}$ is the free-area ratio; δ_{eq} is determined as δ from Eq. (37); k'_{Re} is a function of the Reynolds number, Re, and is estimated from the curve shown in Fig.2, which is fitted by us, from the data(Table 1) provided in [8], to be

$$k'_{Re}=A1+A2\times Re+A3\times Re^2+A4\times Re^3+A5\times Re^4+A6\times Re^5 \tag{40}$$

wherein A1=1.710, A2=-0.6666x10^{-2}, A3=0.2464x10^{-4}, A4=-0.4293x10^{-7}, A5=0.3451x10^{-10}, A6=-0.1028x10^{-13}, Re=Ud/ν, d is the wire diameter , ν is the kinematic viscosity of plain water.

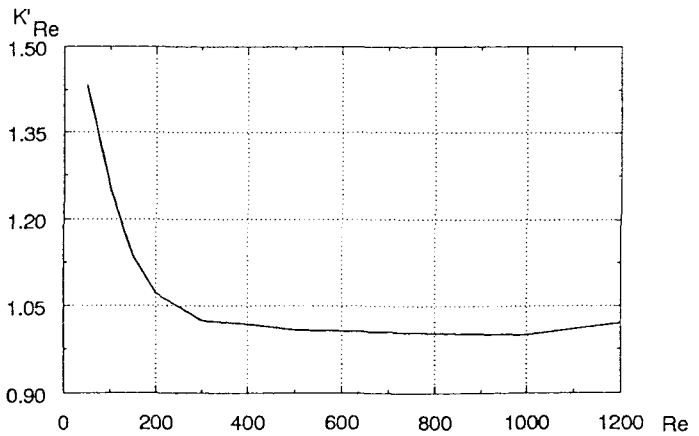

Fig.2 Correction factor of hydraulic resistance for Re<1000

Table 1 Correction factor of hydraulic resistance k'_{Re} vs Reynolds number

Re	5.0	100	150	200	300	400	500	1000	1200
k'_{Re}	1.44	1.24	1.13	1.08	1.03	1.01	1.01	1.01	1.02

The mathematical treatment of the screens is clarified together with the explanation of the finite difference scheme we adopt to discritize the continuum governing equations.

Two staggered meshes displaced with each other by half of one spatial-step, $\Delta x/2$, are defined for the discritization of wave heights and depth-averaged velocities, respectively. This is depicted in Fig.3.

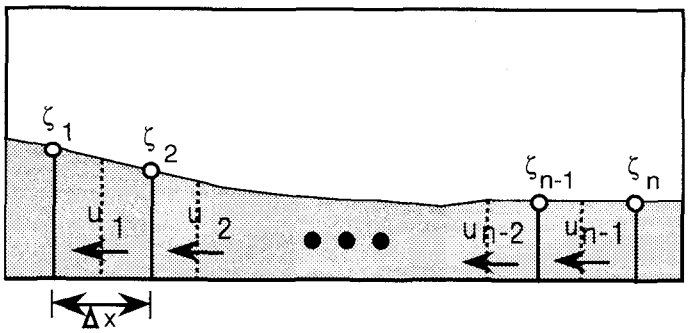

Fig.3. Sketch of the finite difference scheme

In the computation, two sets of simultaneous equations as represented by Eqs. (32), (33), respectively, are solved independently. Eq. (32) stands for a set of simultaneous equations in terms of wave heights while Eq. (33) is for equations with respect to velocities. To mathematically accommodate the effects of one screen, following [6], use is made of the water-head loss, $\Delta\zeta$, which is evaluated from Eq. (35). The velocity, U, passing through the screen is the average of the velocities defined at two mesh points near the screen which are from the computation at the previous time step, i.e, $U=(u_{i-1}+ u_i)/2$. $\Delta\zeta$ is then utilized to modify ζ_i to generate two wave heights, $\zeta_L= \zeta_i + \Delta\zeta/2$, $\zeta_R = \zeta_i - \Delta\zeta/2$, which are actually used to update Eq.(32) before computation is continued to obtain the velocity distribution at the next time level so that the presence of the screen is "felt" or modelled.
The situation involving multiple screen could be dealt with essentially the same way for each individual screen, provided that the screens are spaced approximately above 15 wire diameters or more.

4. RESULTS & COMPARISONS

Notations used in presenting the results are defined first. L=tank length; B=tank width; h=water depth; D=amplitude of base excitation; d=diameter of wires of screens; all wave heights refer to the wave height on an end-wall.

Since we are essentially dealing with resonant motions of water inside rectangular containers, the frequency parameter used in presenting responses is rendered dimensionless with respect to the fundamental frequency, f_w, of water sloshing in a rectangular tank. f_w is evaluated from

$$f_w = \frac{1}{2\pi}\sqrt{\frac{\pi g}{L}\tanh\left(\frac{\pi h}{L}\right)} \qquad \text{(in Hz)}, \tag{41}$$

as is well known, wherein g is the acceleration of gravity.

Useful data of extreme wave heights and total base shear forces from shaking table experiments are provided by the Technical Research Institute of Mitsui Construction Co., Ltd. besides those obtained from the experiments conducted for this study.
For one experimental case, a rectangular tank partially filled with plain water installed with or without screen(s) was driven to experience harmonic, horizontal translation with

single amplitude of D, the steady-state wave height near one end-wall and the total base shear force induced by water sloshing are measured simultaneously, as shown in Fig. 4.

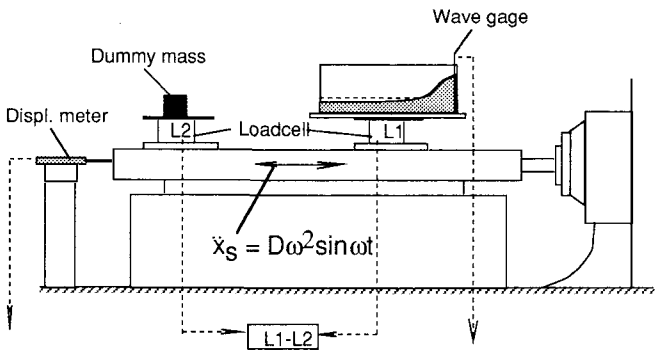

Fig. 4 Experimental set-up

Experimental observations and numerical predictions of frequency responses for both the wave height near one end-wall and the base shear force are presented in a parallel way to facilitate comparison and assessment of the mathematical model. Also displayed are some samples of time-history of wave height and base shear force.

Based on the comparisons, comments will be made on the numerical model. The applicability of the current numerical model is further discussed. Fig.5 presents experimental and theoretical results of wave height for two cases (LxBxh=150x60x37.5cm, expected free-area ratio 51.3%, wire diameter 1.1mm, nondimensional amplitude of excitation D/L= 0.15cm /150cm= 0.001)in the presence of one screen or three screens. Positive extreme wave height is plotted against the forcing frequency of base excitation. The experimental data are provided by the Technical Research Laboratory of Mitsui Construction Co., Ltd.

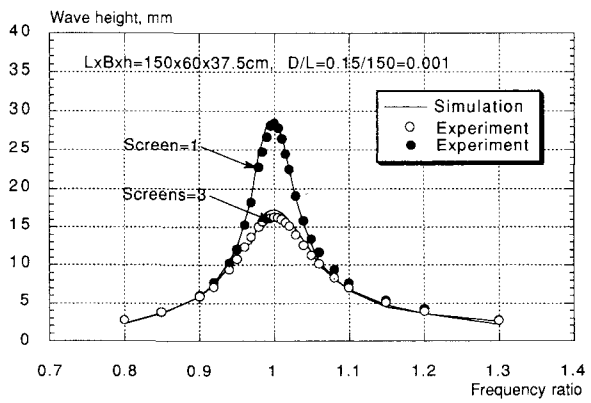

Fig. 5 Frequency response of wave height: Simulations & observations

Numerical predictions compare favorably with experimental observations for these two cases. It should be pointed out, however, that the free-area ratio used in the numerical model is 60% instead of 51.3%, and this value is remained unchanged in the numerical simulations for all cases and good agreements are found. This may justify the

modification of the free-area ratio in the numerical model, because errors might be involved in manufacturing the screens, If the empirical formulas relating the head-loss to the properties of a screen are supposed to be accurate enough.

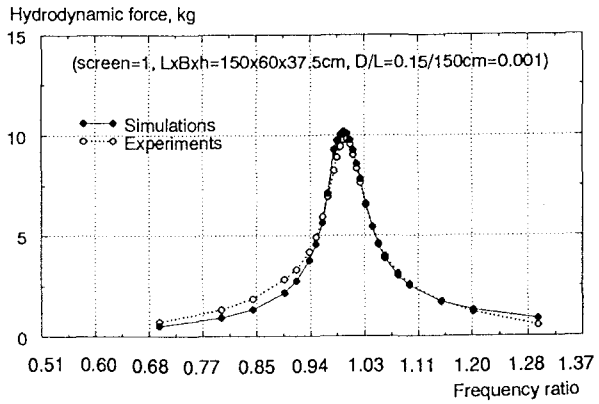

Fig.6 Hydrodynamic forces: Simulations & observations

The frequency response curve of hydrodynamic force corresponding to the curve of one screen in Fig. 5 is depicted in Fig.6, wherein the theoretical estimates are calculated from the wave profile and the contribution of force transmitted to the tank from the screen is also included. Predictions are compared with observations.

Fig. 7 shows the experimental frequency response curves of wave height for three cases studied: 1)Plain water of volume LxBxh=59x33.5x9cm; 2)Plain water of volume LxBxh =59x33.5x9cm with one screen of 70% free-area ratio, wire diameter of 0.6 mm; 3)Plain water of volume LxBxh=59x33.5x9cm with one screen of 50% free-area ratio, wire diameter of 0.4 mm.

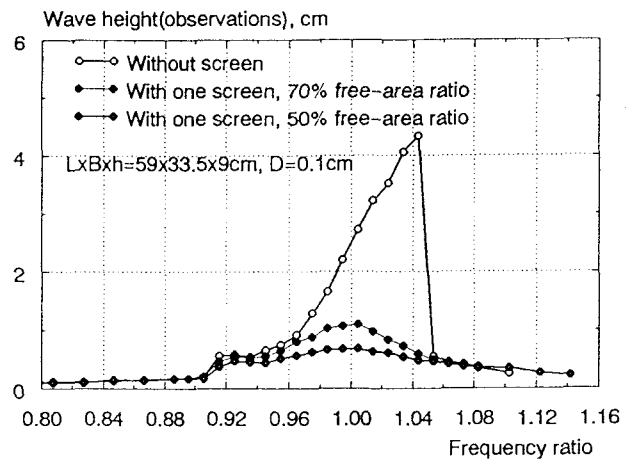

Fig. 7 Frequency response of wave height: Experiments

In Fig.7, the frequency response curve of the case without screen is rather inclined and it assumes a sharp peak at frequency ratio greater than unity. This indicates that the sloshing motions in the case of deeper water is low-damped, nonlinear. The effects of the screen in reducing extreme wave height at resonance, augmenting damping and weakening nonlinearity of water sloshing could be clearly seen by simply comparing the curve forms illustrated in the same figure.

Fig.8 shows the comparison between experimental observations and numerical predictions of the frequency response curves of wave height for case LxBxh=59x33.5x9cm plain water, the amplitude of base excitation is 0.1cm.

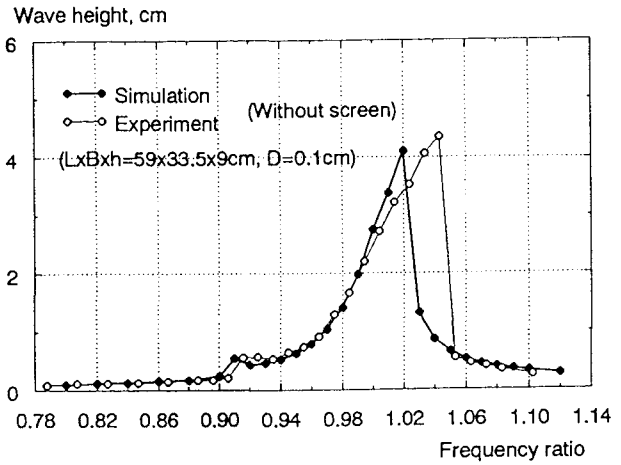

Fig.8 Frequency response of wave height: Simulations & observations

The match between the observations and predictions in this case is not so good as what was shown in Fig. 5 where the relative wave height is much smaller. Larger discrepancy in this case is attributable to the strong nonlinearity accompanying shallow plain water sloshing with larger relative wave amplitude. Because the numerical model is accurate for weakly nonlinear wave motion with small amplitudes and the accuracy is expected to worsen with increasing wave height and stronger nonlinearity.

Samples of time-history of wave height and hydrodynamic force are displayed in Fig.6. Agreements in the time domain are judged to be fairy good as well.

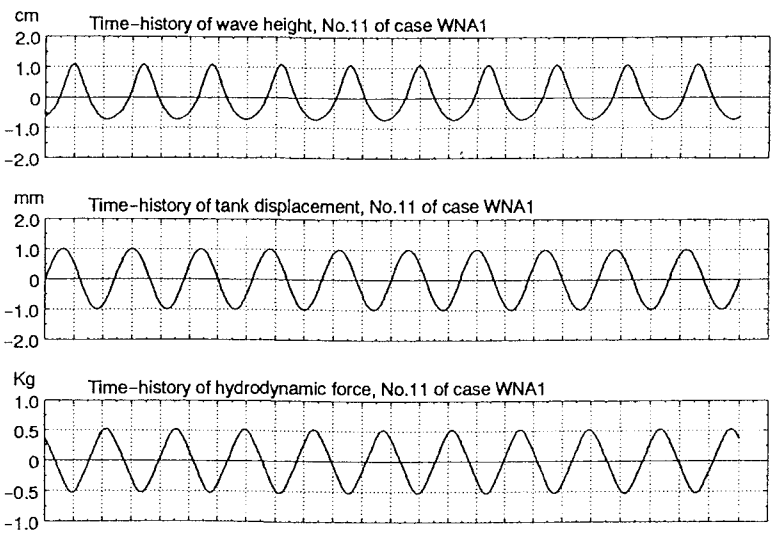

(a)Simulations

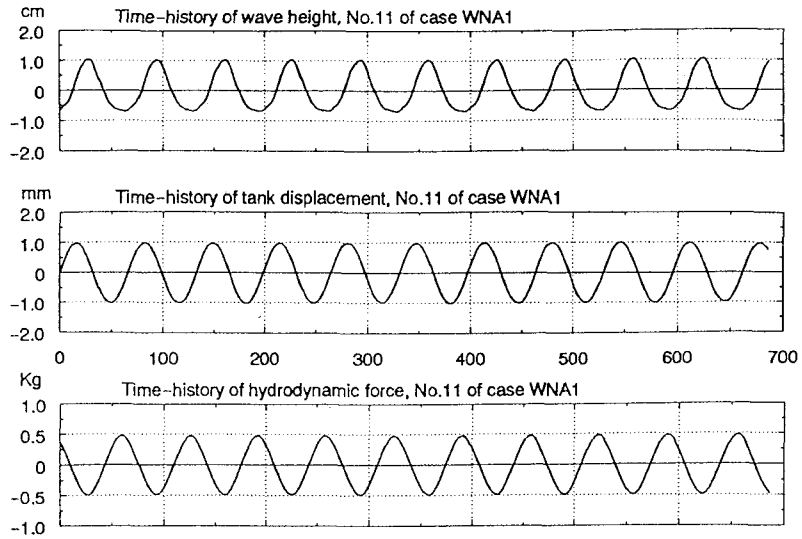

(b)Experiments

Fig.9 Samples of time-histories of wave height and hydrodynamic force

5. DISCUSSIONS

Nonlinearity of water sloshing becomes weaker with increasing water-depth ratio and the introduction of screens. This tendency is observed from several aspects:1)time-histories of wave height at a point is rather symmetric with respect to the still water level; 2)frequency response curves of wave height are nearly symmetrical about a vertical line passing the fundamental frequency point; 3)overall damping level, which is evaluated from frequency response curve using half-power(band-width) method, is not so sensitive to the amplitude of base excitation compared with very shallow water wave motions. This is shown in Fig.10; 3)frequencies at which maximum wave heights occur in the response curves remain almost constant against varying amplitude of base excitation for deeper-water wave motions while they change significantly for wave motions of very shallow water-depth, Fig.11.

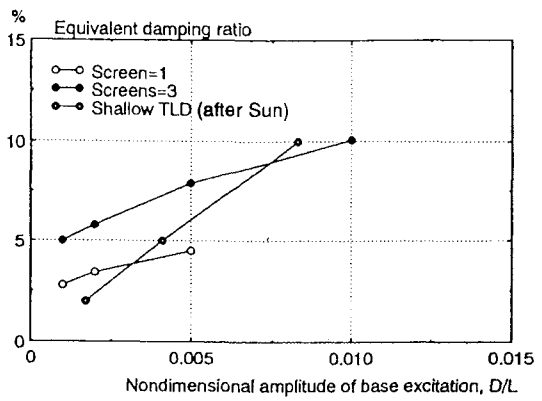

Fig. 10 Nonlinearity of water sloshing: Damping ratio vs amplitude of excitation

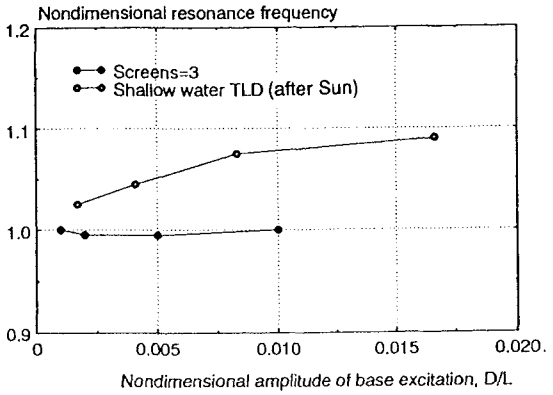

Fig. 11 Nonlinearity of water sloshing: Resonance frequency vs amplitude of excitation

6. CONCLUDING REMARKS

1) Wave motions in rectangular TLD tanks installed with screens could be simulated by the present model with good accuracy provided that the relative extreme wave heights at resonance are small;
2)The accuracy of the numerical model decreases with increasing extreme wave height, and this is theoretically expected from the applicability of the governing equations and confirmed by the outcomes of the predictions;
3)Nonlinearity of water sloshing is weakened considerably with deeper-water and due to the presence of screens;
4)The metal screens are very effective in augmenting the damping of water sloshing. The presence of screens attenuates the nonlinearity of liquid motion.

ACKNOWLEDGEMENTS

The writers of this paper wish to thank DR. Noji of the Technical Research Institute of Mitsui Construction Co., Ltd. for providing very useful experimental data.

REFERENCES

1)Sato, T., *Tuned Sloshing Damper*, Journal of Wind Engineering, JSCE No. 32, May 1987, pp. 67-68.
2)Fujino, Y., and L.M. Sun, *Tuned Liquid damper(TLD) for Suppressing Horizontal Motion of Structures*, J. Eng. Mech., ASCE, October 1992.
3)Sun L., *Semi-analytical modelling of tuned liquid damper(TLD) with emphasis on damping of liquid sloshing*, doctoral dissertation, University of Tokyo, Sep., 1991.
4)Noji T. et al, *Study of water-sloshing vibration control damper(part 1)*, J. Struct. Constr. Eng., AIJ, No. 411, May 1990.
5)Noji T. et al, *Study of vibration control damper using sloshing of water*, J. Struct. Constr. Eng., AIJ, No. 419, Jan., 1991
6)Kaneko, S., and M. Ishikawa, Modelling of tuned liquid damper with submerged nets, AMD-Vol. 151/PVP-Vol. 247, Symposium on flow-induced vibration and noise-Volume 7, ASME 1992.
7) Mei, C. C., *The Applied Dynamics of Ocean Surface Waves*, World Scientific, 1989.
8)Idelchik, I.E., *Handbook of Hydraulic Resistance*, second edition, revised and augmented, Hemisphere Publishing Corporation, 1986.
9)Miles, J.W., *Surface Wave Damping in Closed Basins*, Proc. Royal Society of London, A297, 1967, pp. 459-475.

(Received September 21, 1992)